PLOS ONE

RESEARCH ARTICLE

Fractional integral-like processing in retinal cones reduces noise and improves adaptation

Antal Martinecz¤*, **Mihoko Niitsuma**

Department of Precision Mechanics, Chuo University, Tokyo, Japan

¤ Current address: Department of Pharmacy, University of Tromsø, Tromsø, Norway
* antal.martinecz@uit.no

Abstract

In the human retina, rod and cone cells detect incoming light with a molecule called rhodopsin. After rhodopsin molecules are activated (by photon impact), these molecules activate the rest of the signalling process for a brief period of time until they are deactivated by a multistage process. First, active rhodopsin is phosphorylated multiple times. Following this, they are further inhibited by the binding of molecules called arrestins. Finally, they decay into opsins. The time required for each of these stages becomes progressively longer, and each stage further reduces the activity of rhodopsin. However, while this deactivation process itself is well researched, the roles of the above stages in signal (and image) processing are poorly understood. In this paper, we will show that the activity of rhodopsin molecules during the deactivation process can be described as the fractional integration of an incoming signal. Furthermore, we show how this affects an image; specifically, the effect of fractional integration in video and signal processing and how it reduces noise and the improves adaptability under different lighting conditions. Our experimental results provide a better understanding of vertebrate and human vision, and why the rods and cones of the retina differ from the light detectors in cameras.

Citation: Martinecz A, Niitsuma M (2018) Fractional integral-like processing in retinal cones reduces noise and improves adaptation. PLoS ONE 13(10): e0205099. https://doi.org/10.1371/journal.pone.0205099

Editor: Xiao-Jun Yang, China University of Mining and Technology, CHINA

Received: January 27, 2018

Accepted: August 21, 2018

Published: October 4, 2018

Data Availability Statement: All relevant data are available within the manuscript.

Funding: The author(s) received no specific funding for this work.

Competing interests: The authors have declared that no competing interests exist.

Introduction

As humans rely heavily on visual perception, research on human vision is currently receiving particularly strong interest. Thus, the rods and cones of the retina became among the most well researched cells in human physiology. However, despite the rich literature and constant progress in this field, human vision is still not understood in its entirety owing to its overall complexity [1–5]. This fact is well illustrated by the different scales of interactions that are required to produce a signal in the retina: (i) molecular processes within the photoreceptor cells [6–8]; (ii) the various roles of the photoreceptor cells [9, 10]; (iii) their interactions with other cells before the signal leaves the retina [11–13].

In this paper, we focus on the first step of the signal forming process of rods and cones: the activation and deactivation of rhodopsin. These proteins enter their active state upon impact with a photon, which in turn activates the rest of the signalling cascade until they are deactivated by a multistage process. Each stage of the deactivation process greatly reduces their

activity; however, the time required to complete each step progressively increases, resulting in the temporary accumulation of partially deactivated rhodopsin molecules that still show some residual activity. It is currently unclear whether (and how) these residual activities affect the signal produced by the cell.

During a previous conference, we reported (as preliminary results) that the structure of this process has the potential to approximate the mathematical operations of fractional integration. [14]. Furthermore, we have also shown that the phosphorylation process can approximate this kind of behaviour, based on the commonly used models of the cones [15–17].

Fractional integrals generalise traditional Riemann integrals by allowing integration of non-integer times (e.g. half-integrals). Fractional calculus, which also encompasses fractional integrals, has many interesting real-world applications in various fields, such as robotics [18], modelling ground water pollution [19], modelling drug diffusion in the human body [20], modelling the dynamics of neurons [21], and modelling protein dynamics [22]. Moreover, fractional calculus has been gaining traction in, and proved to be a useful tool for, our topic of interest: image and signal processing [23–25].

In this paper, we investigate whether the multi-stage deactivation process of rhodopsin and related residual activities offer any signal processing benefits, and how it affects signals in general. In our previous work, we used the model presented in [15] to show that this process has the potential to approximate fractional integral-like behaviour. To investigate the effect of the deactivation process, we have expanded this model with the activity of arrestin bound rhodopsin, as it was not previously included.

In addition, we show that the activity of rhodopsin still approximates fractional integration after the addition of the arrestin binding process to the cone model. Furthermore, the addition of the arrestin binding process model expands the frequency range of the approximation. Our main purpose for including these results is to demonstrate that residual activities can accumulate in signalling processes; therefore, they should not be neglected. Finally, as the activity itself can be described as fractional integration, its effects can be predicted without explicitly modelling the process.

Materials and methods

Mathematical model

Active rhodopsin is constantly deactivated by the following process: first, rhodopsin is phosphorylated 5-7 times in rapid succession; following this, it is inhibited by arrestin before finally decaying into opsins within the next few seconds [26–29]. Phosphorylation rates exponentially decrease with each successive phosphorylation: $\gamma_i \approx \gamma \cdot 0.9^i$, where γ, is the rate of the first phosphorylation [15]. However, the rate of arrestin binding linearly increases with each phosphorylation: $\beta_i \approx i \cdot 0.5$, where β_i, is the rate of arrestin binding to rhodopsin phosphorylated i times. This process is described and modelled in detail in [15–17], which we used as a foundation for our model (Eqs 1a–1d). We extended the model by adding the stage where rhodopsin is inhibited by arrestin, and retains only a fraction of its original activity (Eq 1e) [10, 30–33]. With each phosphorylation, rhodopsin is inhibited by 50% [15], and the binding of arrestin further inhibits activity by a = 50–90% [30–32].

The equations of the model for 6 phosphorylations are as follows:

$$\dot{r}_0 = \text{input}(t) - \gamma_0 r_0 \tag{1a}$$

$$\dot{r}_1 = \gamma_0 r_0 - (\gamma_1 + \beta_1) r_1 \tag{1b}$$

$$\begin{aligned} \dot{r}_2 &= \gamma_1 r_1 - (\gamma_2 + \beta_2) r_2 \\ &\vdots \end{aligned} \tag{1c}$$

$$\dot{r}_6 = \gamma_5 r_5 - \beta_6 r_6 \tag{1d}$$

$$\dot{r}_{arr} = \sum_{i=0}^{6} \beta_i r_i - 0.3 r_{arr}, \tag{1e}$$

where r_i is the number of rhodopsin molecules with levels of phosphorylation and r_{arr} is the number of rhodopsin molecules bound by arrestin. The total activity of the rhodopsin is the output of the model, as follows:

$$\text{output(t)} = \sum_{i=0}^{6} 2^{-i} r_i + 2^{-6} \cdot a \cdot r_{arr} \tag{2}$$

The arrestin binding rates for the intermediate phosphorylation steps are of little significance, as the phosphorylation rates are a magnitude faster. Therefore, as previously reported in [14], the system of equations can be simplified without affecting the output. Fig 1 shows that the impulse responses were approximately the same before and after simplification. As these are linear systems of equations, estimating the impulse response was sufficient for approximation.

The simplified equations are as follows:

$$\dot{r}_0 = \text{input}(t) - \gamma_5 r_0 \tag{3a}$$

$$\dot{r}_6 = \gamma_5 r_0 - \beta_6 r_6 \tag{3b}$$

$$\dot{r}_{arr} = \beta_6 r_6 - 0.3 r_{arr}, \tag{3c}$$

In this case the output is:

$$\text{output(t)} = r_0 + 2^{-6} r_6 + 2^{-6} a \cdot r_{arr} \tag{4}$$

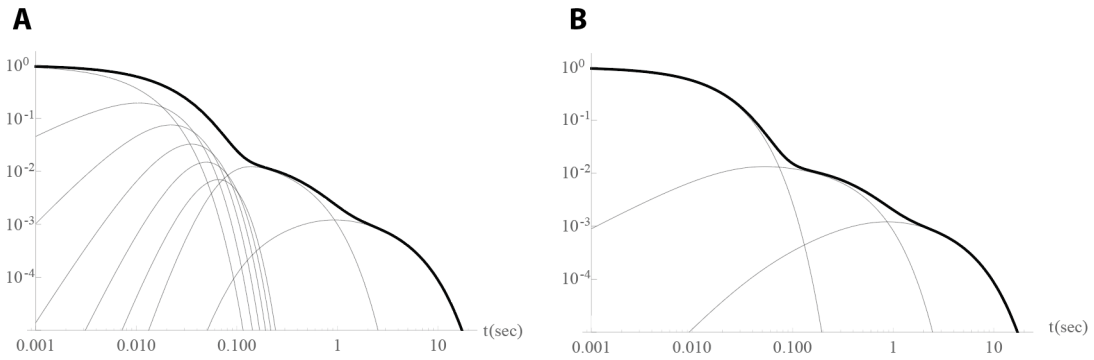

Fig 1. Impulse responses of full (panel A, Eqs 1 and 2) and simplified model (panel B, Eqs 3 and 4). The thin lines are the contributions of the individual equations to the output (black curves).

https://doi.org/10.1371/journal.pone.0205099.g001

Fractional integrals

Definition

Fractional integrals require multiple definitions, approximations, and numerical methods to solve [34–39]. Here, we used the Riemann-Liouville definition expressed with a convolution operation [40] as the definition, which shows the impulse response of the operation. In this paper, we show how this impulse response was approximated by the deactivation of rhodopsin in response to a single impulse of light.

$$\mathrm{I}^{\alpha} f(t) = f(t) \otimes \left(\frac{1}{\Gamma(\alpha)} t^{\alpha-1}\right). \tag{5}$$

The above equation is a linear operation with an impulse response of $\frac{1}{\Gamma(\alpha)} t^{\alpha-1}$, where $\Gamma(\alpha)$ is the gamma function and the generalisation of the factorials.

Approximation

As mentioned above, linear operations and systems are fully defined by their impulse responses. A system whose impulse response approximates the impulse response of a fractional integral will also approximate the fractional integral itself. Similar to results reported in [14] and [21], we have shown that connected feedback loops with logarithmically decreasing poles (Eqs 6–9) can be used to approximate fractional integrals, and the sum of their weighted responses approximates the response of the fractional integrals. (see Fig 2).

With differential equations:

$$\dot{x}_0 = f(t) - c x_0 \tag{6}$$

$$\dot{x}_1 = c x_0 - c^2 x_1 \tag{7}$$

$$\begin{aligned} \dot{x}_2 &= c^2 x_1 - c^3 x_2, \\ &\vdots \end{aligned} \tag{8}$$

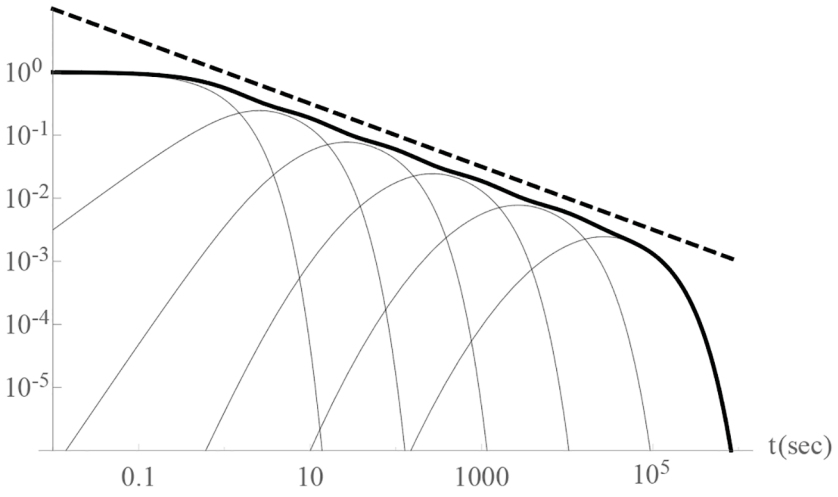

Fig 2. Approximation (solid black curve, Eqs 6–9) of a half integral's ($\mathrm{I}^{0.5}$) impulse response: $t^{-0.5}$ (dashed line) on the log–log plot. The grey lines represent each feedback loop's contribution to the output.

https://doi.org/10.1371/journal.pone.0205099.g002

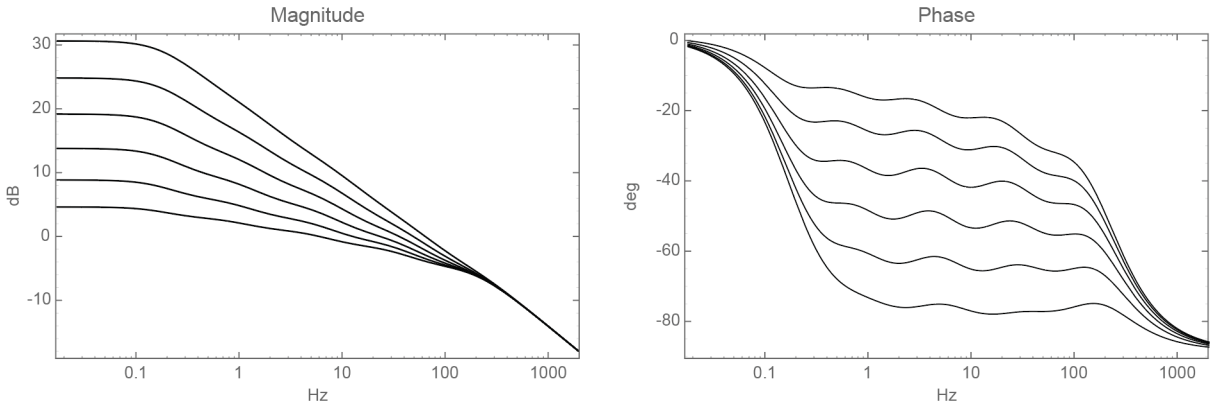

Fig 3. Bode plots of approximations to fractional integrals: $I^{0.15}$, $I^{0.3}$, $I^{0.45}$, $I^{0.6}$, $I^{0.75}$, $I^{0.9}$ (Eqs 6–9).

https://doi.org/10.1371/journal.pone.0205099.g003

where the output is:

$$\mathrm{I}^{\alpha} f(t) = \sum_{i} (c^{i(1-\alpha)} x_i), \tag{9}$$

and $0 < c < 1$ is the spacing of the feedback loops; for example, $c = 1/10$.

Bode Plots

Bode plots fully define a system by plotting the relationship between the input's frequency and the output's phase and amplification in linear systems. These plots can be used to identify fractional integrals, as a fractional integral I^{α} has a constant phase shift at -90α degrees and an amplification of -20α dB/dec [41].

See examples on the approximation (Eqs 6–9) in Fig 3.

Results and discussion

Activity of rhodopsins approximate a fractional integral

We plotted all the Bode plots (Fig 4) of the model (Eqs 3 and 4) with all the different combinations along with the published parameter ranges of the activation and deactivation rates

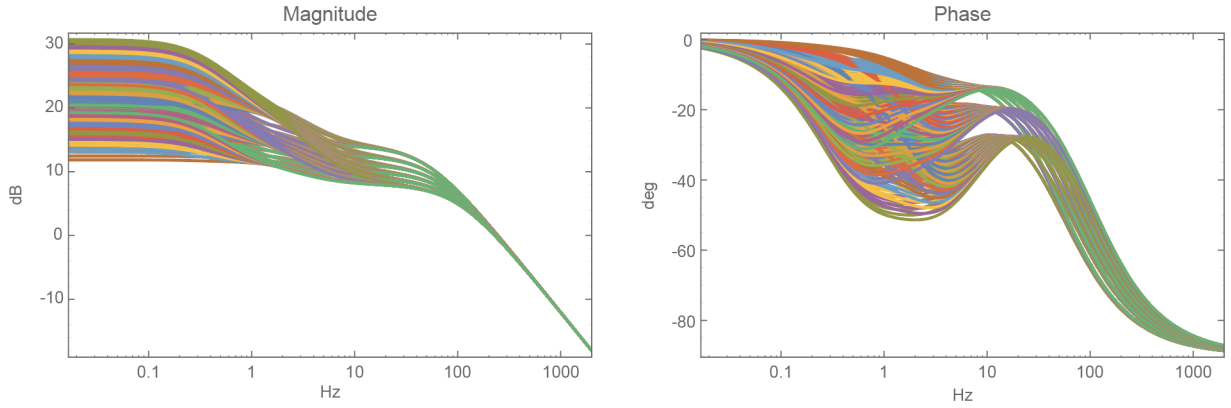

Fig 4. Bode-plots of rhodopsin's activity with the different combinations of parameters found in the literature (number of phosphorylations, phosphorylation rate, inhibition by arrestin). In most of these cases, the phase-shift plots plateaued between the frequencies of 0.3-30Hz; therefore, we approximated fractional integrals within that range.

https://doi.org/10.1371/journal.pone.0205099.g004

Table 1. Parameters for the rhodopsin's deactivation process.

Parameter	Approximate values	References
Phosphorylation rates	60–90[1/*s*]	[15, 28]
Inhibition per phosphorylation	50%	[15, 28]
Number of phosphorylations	5–7	[15–17, 26]
Arrestin binding rates	2[1/*s*]	[15, 28]
Inhibition by arrestin	50%–99%	[30–32]
Decay rate into opsins	0.3[1/*s*]	[10, 33]

https://doi.org/10.1371/journal.pone.0205099.t001

(Table 1). As with Fig 3, the phase plots plateaued at -90α degrees; specifically, between −9 and −27 degrees. Therefore, the rhodopsin's activity approximated a fractional integration between the orders of 0.1–0.3.

The parameters used for plotting are:

- phosphorylation rates between 50 and 100 1/s with steps of 10 1/s,
- inhibition by the binding of arrestin, between 51% and 99% with the steps of 5%,
- number of phosphorylations: 5, 6 or 7.

Noise reduction and movement

The image produced by rhodopsin molecules can be imagined as a composition of images produced by cameras with different exposure times. Speaking mathematically, simple cameras with different exposure times can be described as a feedback loop where the exposure time corresponds to the time constant of the loop; in our case, the time rhodopsin spends at each deactivation step (see Fig 5).

In signal and image processing, feedback loops are low-pass filters; they suppress high frequency components of the signals. Thus, they are often used to reduce measurement noise.

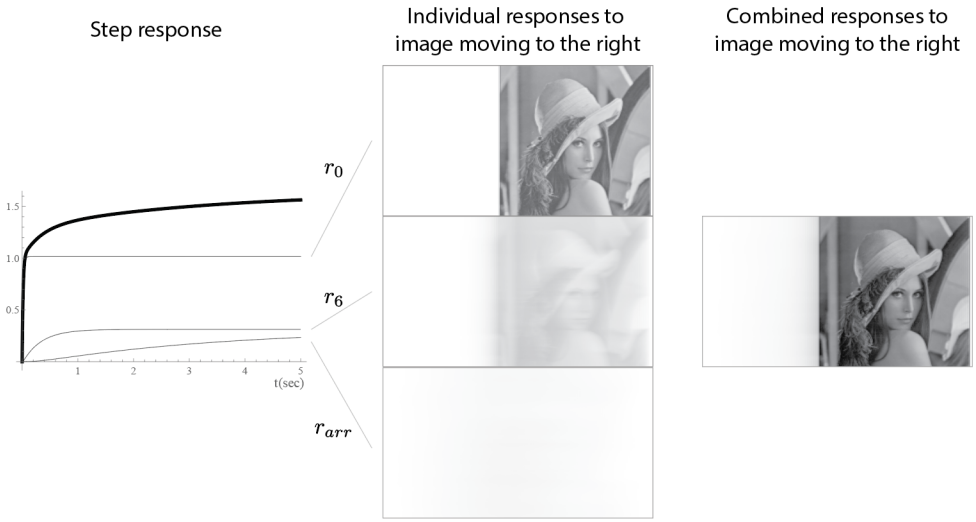

Fig 5. The contribution of the different stages of rhodopsin deactivation to the impulse response. The left side depicts the responses (grey) and their sum (black) to a step input. The middle images show the responses to a video of a moving image at each stage (from left to right). The right side shows the combined images.

https://doi.org/10.1371/journal.pone.0205099.g005

Higher frequency components in video processing are either fast movements or noise; therefore, noise reduction comes with the compromise of losing detail in moving objects. In other words, the faster the movement (higher frequency), the more detail is suppressed and blurred. In noise reduction, fractional integration offers a compromise, as it is a combination of different feedback loops and the high frequency components are kept but are slightly suppressed by the other loops. As a result, the noise reduction and blur effects are more "gentle" than in the case of feedback loops (see Fig 5). This is indicated in the bode-plots with the slope of -20α dB/dec. For cones this is approximately −4 dB/dec); for the first order feedback loops this is −20 dB/dec slope (Fig 4).

We speculate that, as human eyes fixate on objects of interest [42], this kind of processing allows us to visually ignore some of the motion and noise we are not interested in at a given moment. For example, during a snowfall, individual snowflakes do not necessarily disappear from our vision, but are gently suppressed.

Adaptation

In [43], it was shown that adding a power law dynamic to an auditory-nerve and inner hair cell model allowed the adaptive part of the model to adapt to a wider range of signals. Moreover, it showed a possible explanation as to how the neurons in the auditory nerve system can adapt their responses according to input history.

In our case, fractional integrals add power law dynamics to the model, as their impulse response follows power law dynamics. Thus, the response to sustained inputs can reach higher levels than would be possible with only an exponential decay (see Fig 5). In addition, as pupils contract in response to light, the possible magnitudes are restricted (under normal lighting conditions). Therefore, power law dynamics provided by fractional integrals can allow the process to reach higher levels of overall activity in response to sustained inputs that would otherwise be impossible to achieve. This would allow the processes inside and outside cones to adapt to (and differentiate between) lighting conditions and temporarily high input levels.

Conclusions and future directions

We have shown how rhodopsin's ability to activate the rest of the signalling approximates a fractional integral. Furthermore, we have shown how this affects the rest of the signalling process; namely, it improves the cone cells' abilities to adapt to different light conditions and reduces noise in "measuring" the number of incoming photons.

Fractional components allow the fine-tuning of responses in proportional-integral-derivative (PID)-type controllers [44]. We hypothesise that this rhodopsin signalling behaviour confers additional benefits when combined with the full cone model described in [15]. The full cone model can be considered as a PD-type controller that follows a signal with an overshoot. Fig 6 demonstrates the hypothetical cases where the model parameters are insufficient for approximate fractional integration. Furthermore, the subsequent stages in the retina process the signal and transform the it even further into a derivative of the original signal [45–47]. To demonstrate why this is important, we have plotted three cases in addition to a simple feedback loop: (i) approximation, (ii) when the activity of phosphorylated rhodopsin is too low for approximation, and (iii) where it is too high for an approximation. In this specific case, the inclusion of fractional integrals in the model decreases this overshoot while still allowing a rapid response. However, how this specifically affects the rest of the signalling process remains unknown.

Research on image processing based on visual process (such as this paper or [45, 48–50]) help us understand how human vision works and its differences from the cameras and

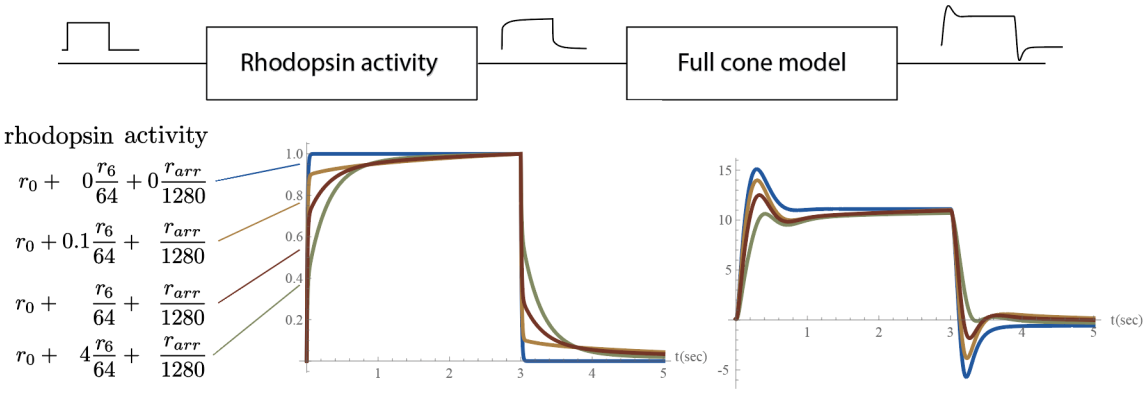

Fig 6. Step responses and responses of the full cone model [15] to them. Blue curves: only r_0. Orange curves: insufficient r_6 activity. Brown curves: approximation to fractional integral. Green curves: excessive r_6 activity.

https://doi.org/10.1371/journal.pone.0205099.g006

detectors used in computer vision. As a result, such research will allow us to improve and develop image processing algorithms, and understand the limitations and advantages of not current algorithms and our own vision.

Acknowledgments

Preliminary results from this work were presented at the 2015 International Conference on Informatics in Control and appear in its proceedings [14].

Author Contributions

Conceptualization: Antal Martinecz.

Investigation: Antal Martinecz.

Project administration: Mihoko Niitsuma.

Supervision: Mihoko Niitsuma.

Writing – original draft: Antal Martinecz.

Writing – review & editing: Mihoko Niitsuma.

References

1. Burns ME, Pugh EN. Lessons from Photoreceptors: Turning Off G-Protein Signaling in Living Cells. Physiology. 2010; 25(2):72–84. https://doi.org/10.1152/physiol.00001.2010 PMID: 20430952
2. Arshavsky VY, Burns ME. Current understanding of signal amplification in phototransduction. Cellular logistics. 2014; 4(May):e29390. https://doi.org/10.4161/cl.29390 PMID: 25279249
3. Marc RE, Jones BW, Lauritzen JS, Watt CB, Anderson JR. Building retinal connectomes. Current Opinion in Neurobiology. 2012; 22(4):568–574. https://doi.org/10.1016/j.conb.2012.03.011 PMID: 22498714
4. Reuter T. Fifty years of dark adaptation 1961-2011. Vision Research. 2011; 51(21-22):2243–2262. https://doi.org/10.1016/j.visres.2011.08.021 PMID: 21925198
5. Hu ZH, Luo X, Chen ZZ. A Computational Model for Processing Object Motion Based on Retina Neural Mechanism. Proceedings of the 2013 International Conference on Advanced Computer Science and Electronics Information. 2013;(Icacsei):692–696.
6. Ascano M, Robinson PR. Differential phosphorylation of the rhodopsin cytoplasmic tail mediates the binding of arrestin and its splice variant, p44. Biochemistry. 2006; 45(7):2398–2407. https://doi.org/10.1021/bi052021h PMID: 16475829

7. Bayburt TH, Vishnivetskiy SA, McLean MA, Morizumi T, Huang CC, Tesmer JJG, et al. Monomeric rhodopsin is sufficient for normal rhodopsin kinase (GRK1) phosphorylation and arrestin-1 binding. Journal of Biological Chemistry. 2011; 286(2):1420–1428. https://doi.org/10.1074/jbc.M110.151043 PMID: 20966068
8. Gross OP, Pugh EN Jr, Burns ME. cGMP in mouse rods: the spatiotemporal dynamics underlying single photon responses. Frontiers in Molecular Neuroscience. 2015; 8(March):1–10.
9. Ingram NT, Sampath AP, Fain GL. Why are rods more sensitive than cones? Journal of Physiology. 2016; 594(19):5415–5426. https://doi.org/10.1113/JP272556 PMID: 27218707
10. Shi G, Yau KW, Chen J, Kefalov VJ. Signaling Properties of a Short-Wave Cone Visual Pigment and Its Role in Phototransduction. Journal of Neuroscience. 2007; 27(38):10084–10093. https://doi.org/10.1523/JNEUROSCI.2211-07.2007 PMID: 17881515
11. Babai N, Thoreson WB. Horizontal cell feedback regulates calcium currents and intracellular calcium levels in rod photoreceptors of salamander and mouse retina. Journal of Physiology. 2009; 587(10):2353–2364. https://doi.org/10.1113/jphysiol.2009.169656 PMID: 19332495
12. Awatramani GB, Slaughter MM. Origin of Transient and Sustained Responses in Ganglion Cells of the Retina. Journal of Neuroscience. 2000; 20(18):7087–7095. https://doi.org/10.1523/JNEUROSCI.20-18-07087.2000 PMID: 10995856
13. Werblin FS. The retinal hypercircuit: A repeating synaptic interactive motif underlying visual function. Journal of Physiology. 2011; 589(15):3691–3702. https://doi.org/10.1113/jphysiol.2011.210617 PMID: 21669978
14. Martinecz A, Niitsuma M. Modeling the G-Protein Signaling of the Retina with Fractional Calculus. In: Proceedings of the 12th International Conference on Informatics in Control, Automation and Robotics. SCITEPRESS—Science and and Technology Publications; 2015. p. 481–488.
15. Korenbrot JI. Speed, adaptation, and stability of the response to light in cone photoreceptors: The functional role of Ca-dependent modulation of ligand sensitivity in cGMP-gated ion channels. The Journal of General Physiology. 2012; 139(1):31–56. https://doi.org/10.1085/jgp.201110654 PMID: 22200947
16. Dell'Orco D, Schmidt H, Mariani S, Fanelli F. Network-level analysis of light adaptation in rod cells under normal and altered conditions. Molecular bioSystems. 2009; 5(10):1232–1246. https://doi.org/10.1039/b908123b PMID: 19756313
17. Hamer RD, Nicholas SC, Tranchina D, Lamb TD, Jarvinen JLP. Toward a unified model of vertebrate rod phototransduction. Visual Neuroscience. 2005; 22(4):417–436. https://doi.org/10.1017/S0952523805224045 PMID: 16212700
18. Coronel-Escamilla A, Torres F, Gómez-Aguilar JF, Escobar-Jiménez RF, Guerrero-Ramírez GV. On the trajectory tracking control for an SCARA robot manipulator in a fractional model driven by induction motors with PSO tuning. Multibody System Dynamics. 2017;
19. Atangana A, Alqahtani RT. Numerical approximation of the space-time Caputo-Fabrizio fractional derivative and application to groundwater pollution equation. Advances in Difference Equations. 2016; 2016(1):156. https://doi.org/10.1186/s13662-016-0871-x
20. Chevalier A, Copot D, Ionescu CM, De Keyser R. Fractional order impedance models as rising tools for quantification of unconscious analgesia. 2013 21st Mediterranean Conference on Control and Automation, MED 2013—Conference Proceedings. 2013; p. 206–212.
21. Anastasio TJ. The fractional-order dynamics of brainstem vestibulo-oculomotor neurons. Biological Cybernetics. 1994; 72(1):69–79. https://doi.org/10.1007/BF00206239 PMID: 7880915
22. Glöckle WG, Nonnenmacher TF. A fractional calculus approach to self-similar protein dynamics. Biophysical Journal. 1995; 68(1):46–53. https://doi.org/10.1016/S0006-3495(95)80157-8 PMID: 7711266
23. Bai J, Feng XC. Fractional-Order Anisotropic Diffusion for Image Denoising. IEEE Transactions on Image Processing. 2007; 16(10):2492–2502. https://doi.org/10.1109/TIP.2007.904971 PMID: 17926931
24. Cuesta E, Kirane M, Malik SA. Image structure preserving denoising using generalized fractional time integrals. Signal Processing. 2012; 92(2):553–563. https://doi.org/10.1016/j.sigpro.2011.09.001
25. Das S, Pan I. Fractional Order Signal Processing. 2012; p. 13–31.
26. Lamb TD, Pugh EN. Dark adaptation and the retinoid cycle of vision. Progress in Retinal and Eye Research. 2004; 23(3):307–380. https://doi.org/10.1016/j.preteyeres.2004.03.001 PMID: 15177205
27. Wang JS, Kefalov VJ. The Cone-specific visual cycle; 2011.
28. Korenbrot JI. Speed, sensitivity, and stability of the light response in rod and cone photoreceptors: Facts and models. Progress in Retinal and Eye Research. 2012; 31(5):442–466. https://doi.org/10.1016/j.preteyeres.2012.05.002 PMID: 22658984

29. Yau KW, Hardie RC. Phototransduction Motifs and Variations. Cell. 2009; 139(2):246–264. https://doi.org/10.1016/j.cell.2009.09.029 PMID: 19837030

30. Krupnick JG, Gurevich VV, Benovic JL. Mechanism of quenching of phototransduction: Binding competition between arrestin and transducin for phosphorhodopsin. Journal of Biological Chemistry. 1997; 272(29):18125–18131. https://doi.org/10.1074/jbc.272.29.18125 PMID: 9218446

31. Sinha A, Jones Brunette AM, Fay JF, Schafer CT, Farrens DL. Rhodopsin TM6 can interact with two separate and distinct sites on arrestin: Evidence for structural plasticity and multiple docking modes in arrestin-rhodopsin binding. Biochemistry. 2014; 53(20):3294–3307. https://doi.org/10.1021/bi401534y PMID: 24724832

32. Golobokova EY, Govardovskii VI. Late stages of visual pigment photolysis in situ: Cones vs. rods. Vision Research. 2006; 46(14):2287–2297. https://doi.org/10.1016/j.visres.2005.12.017 PMID: 16473387

33. Vishnivetskiy SA, Paz CL, Schubert C, Hirsch JA, Sigler PB, Gurevich VV. How does arrestin respond to the phosphorylated state of rhodopsin? Journal of Biological Chemistry. 1999; 274(17):11451–11454. https://doi.org/10.1074/jbc.274.17.11451 PMID: 10206946

34. Atangana A, Gómez-Aguilar JF. Numerical approximation of Riemann-Liouville definition of fractional derivative: From Riemann-Liouville to Atangana-Baleanu. Numerical Methods for Partial Differential Equations. 2017;

35. Atangana A, Nieto JJ. Numerical solution for the model of RLC circuit via the fractional derivative without singular kernel. Advances in Mechanical Engineering. 2015; 7(10):168781401561375. https://doi.org/10.1177/1687814015613758

36. Yépez-Martínez H, Gómez-Aguilar JF, Sosa IO, Reyes JM, J TJ. The Feng's first integral method applied to the nonlinear mKdV space-time fractional partial differential equation. Revista Mexicana de Física. 2016; 62(4):310–316.

37. Gómez-Aguilar J, Yépez-Martínez H, Torres-Jiménez J, Córdova-Fraga T, Escobar-Jiménez R, Olivares-Peregrino V. Homotopy perturbation transform method for nonlinear differential equations involving to fractional operator with exponential kernel. Advances in Difference Equations. 2017; 2017(1):68. https://doi.org/10.1186/s13662-017-1120-7

38. Coronel-Escamilla A, Gómez-Aguilar J, Baleanu D, Córdova-Fraga T, Escobar-Jiménez R, Olivares-Peregrino V, et al. Bateman–Feshbach Tikochinsky and Caldirola–Kanai Oscillators with New Fractional Differentiation. Entropy. 2017; 19(2):55. https://doi.org/10.3390/e19020055

39. Morales-Delgado VF, Gómez-Aguilar JF, Yépez-Martínez H, Baleanu D, Escobar-Jimenez RF, Olivares-Peregrino VH. Laplace homotopy analysis method for solving linear partial differential equations using a fractional derivative with and without kernel singular. Advances in Difference Equations. 2016; 2016(1):164. https://doi.org/10.1186/s13662-016-0891-6

40. Podlubny I. Fractional-Order Systems and -PID Controllers. IEEE Transactions on Automatic Control. 1999; 44(1):208–214. https://doi.org/10.1109/9.739144

41. Vinagre B M, Podlubny I, Hernandez A, Feliu V. Some Approximations of Fractional Order Operators used in Control Theory and Applications. Fractional Calculus & Applied Analysis. 2000; 3(3):231–248.

42. Tatler BW, Wade NJ, Kwan H, Findlay JM, Velichkovsky BM. Yarbus, eye movements, and vision. i-Perception. 2010; 1(1):7–27. https://doi.org/10.1068/i0382 PMID: 23396904

43. Zilany MSA, Carney LH. Power-Law Dynamics in an Auditory-Nerve Model Can Account for Neural Adaptation to Sound-Level Statistics. Journal of Neuroscience. 2010; 30(31):10380–10390. https://doi.org/10.1523/JNEUROSCI.0647-10.2010 PMID: 20685981

44. Shah P, Agashe S. Review of fractional PID controller. Mechatronics. 2016; 38:29–41. https://doi.org/10.1016/j.mechatronics.2016.06.005

45. Ichinose T, Fyk-Kolodziej B, Cohn J. Roles of ON Cone Bipolar Cell Subtypes in Temporal Coding in the Mouse Retina. Journal of Neuroscience. 2014; 34(26):8761–8771. https://doi.org/10.1523/JNEUROSCI.3965-13.2014 PMID: 24966376

46. van Hateren H. A cellular and molecular model of response kinetics and adaptation in primate cones and horizontal cells. Journal of Vision. 2005; 5(4):5. https://doi.org/10.1167/5.4.5

47. Crook JD, Manookin MB, Packer OS, Dacey DM. Horizontal Cell Feedback without Cone Type-Selective Inhibition Mediates "Red-Green" Color Opponency in Midget Ganglion Cells of the Primate Retina. Journal of Neuroscience. 2011; 31(5):1762–1772. https://doi.org/10.1523/JNEUROSCI.4385-10.2011 PMID: 21289186

48. Devillard F, Heit B, Others. Architectural Model of a Biological Retina Using Cellular Automata. Journal of Computer and Communications. 2014; 2(14):78. https://doi.org/10.4236/jcc.2014.214008

49. Yang K, Gao S, Li C, Li Y. Efficient Color Boundary Detection with Color-Opponent Mechanisms. 2013 IEEE Conference on Computer Vision and Pattern Recognition. 2013; p. 2810–2817.

50. Gould S, Arfvidsson J, Kaehler A, Sapp B, Messner M, Bradski GR, et al. Peripheral-Foveal Vision for Real-time Object Recognition and Tracking in Video. In: Ijcai. vol. 7. Morgan Kaufmann Publishers Inc.; 2007. p. 2115–2121.